

Showcasing research from Dr Ryo Tsunashima's laboratory,
Graduate School of Science and Engineering for Innovation,
Yamaguchi University, Yamaguchi, Japan

Solvent-assisted mechanochemical crystallization of the
metal-free perovskite solid solution $(\text{H}_2\text{dabco}, \text{H}_2\text{hmta})\text{NH}_4(\text{BF}_4)_3$

Solid solution of metal-free perovskite was crystallized using
a solvent-assisted mechanochemical process at a wide range
of dabco : hmta ratios.

As featured in:



See Ryo Tsunashima *et al.*,
Chem. Commun., 2024, **60**, 12181.



Cite this: *Chem. Commun.*, 2024, 60, 12181

Received 7th August 2024,
Accepted 28th August 2024

DOI: 10.1039/d4cc04010d

rsc.li/chemcomm

All-proportional solid solutions of the metal-free perovskite $(H_2dabco_{1-y} H_2hmta_y)(NH_4)(BF_4)_3$ ((d,h)-BF₄**) were crystallized via a mechanochemical method. Their molecular dynamics depend on the ratio y with a compositional boundary at $y = 0.43$, where H_2dabco^{2+} was deduced to be at a dynamic disorder state, even below phase transition temperature to a plastic crystalline phase seen at $y = 0$.**

Perovskite-type oxides in functional materials such as ferroelectrics and piezoelectrics are often found in solid solution.^{1,2} This is because their chemical and physical properties can be finely controlled by a combination and ratio of metal ions. A solid solution with different structural symmetries also exhibits unique physical properties related to structural instability at the compositional boundary of components, known as a morphotropic phase boundary, such as lead zirconate titanate.^{3–5}

In 2002, the third type of ABX_3 perovskite structures was reported, followed by traditional fully inorganic perovskites and organic–inorganic hybrid perovskites.⁶ Both A-sites and B-sites are occupied by molecular ions instead of metals, in what are known as metal-free molecular perovskites. In 2018, ferroelectricity was realized using non-centrosymmetric organic molecules at the A-site.⁷ Successive reports have described the properties of these materials, including visible luminescence with high fluorescence quantum yields, and X-ray detection.^{8–12}

^a Graduate School of Sciences and Technology for Innovation, Yamaguchi University, Yoshida 1677-1, Yamaguchi, 753-8512, Japan.

E-mail: ryotsuna@yamaguchi-u.ac.jp

^b Chemistry Course, Faculty of Science, Yamaguchi University, Yoshida 1677-1, Yamaguchi, 753-8512, Japan

^c Graduate School of Advanced Science and Engineering, Hiroshima University, Higashi-Hiroshima 739-8526, Japan

^d Institute of Multidisciplinary Research for Advanced Materials (IMRAM), Tohoku University, Sendai 980-8577, Japan

† Electronic supplementary information (ESI) available: Method, FT-IR spectra, TG-DTA, LC-MS, DSC, powder X-ray diffraction, complex permittivity, and solid-state ¹³C-NMR. CCDC 2347881 and 2347882. For ESI and crystallographic data in CIF or other electronic format see DOI: <https://doi.org/10.1039/d4cc04010d>

Solvent-assisted mechanochemical crystallization of the metal-free perovskite solid solution $(H_2dabco, H_2hmta)NH_4(BF_4)_3$ †

Jumpei Moriguchi,^a Tomoe Koga,^b Nao Tsunooji,^c Sadafumi Nishihara,^c Tomoyuki Akutagawa,^d Atsuko Masuya-Suzuki^{ab} and Ryo Tsunashima^{ab}

These materials have advantageous qualities with respect to reduced effects on humans and the environment more broadly.

Spontaneous polarization of perovskites is often caused by distortion of the $\{BX_6\}$ octahedron. Unlike metal-containing systems however, whose distortion usually originates from metal ions via the pseudo-Jahn–Teller effect, the $\{(NH_4)X_6\}$ octahedron in metal-free perovskites does not have a mechanism for spontaneous polarization. Both polarization and dielectric properties are affected by the characteristics of the interaction, steric hindrances, symmetry, and orientation of the A-site molecule.

We have investigated solid solutions of A-site molecules with different characteristics: hexamethylenetetramine (hmta) and 1,4-diazabicyclo[2.2.2]octane (dabco). In the perovskite structure, non-centrosymmetric $(H_2hmta)(NH_4)Br_3$ (**h-Br**)¹³ was mixed with centrosymmetric $(H_2dabco)(NH_4)Br_3$ (**d-Br**), resulting in the solid solution $(H_2dabco, H_2hmta)(NH_4)Br_3$ (**(d,h)-Br**). Unlike **d-Br**, which underwent a first-order type phase transition to a plastic crystalline (PC) phase at 327 K,⁷ a second-order type transition with Debye-type dielectric relaxation at approximately 200 K was observed for **(d,h)-Br**. It was considered that H_2hmta^{2+} induced structural fluctuations in the lattice that activate the thermal motion of surrounding H_2dabco^{2+} .¹⁴ However, the solid solution was crystallized from an aqueous solution, and hmta was only miscible below a few mol% due to hydrolysis in the acidified aqueous solution.

Mechanochemical methods^{15–22} are techniques for reacting components via mechanical processes such as compression and shearing. This can facilitate products and reactions that differ from those associated with solution-based synthesis.^{15–17} Metal-free perovskites have been crystallized via mechanochemical methods.¹⁸ Additionally, mechanochemical methods have been used to achieve solid solutions of species that are difficult to mix in solution or the liquid phase.^{19–22}

The present study investigated the use of mechanochemical methods to crystallize solid solutions of the metal-free perovskite crystals between $(H_2hmta)(NH_4)(BF_4)_3$ (**h-BF₄**) and $(H_2dabco)(NH_4)(BF_4)_3$ (**d-BF₄**). The phase transition of **d-BF₄** was reported



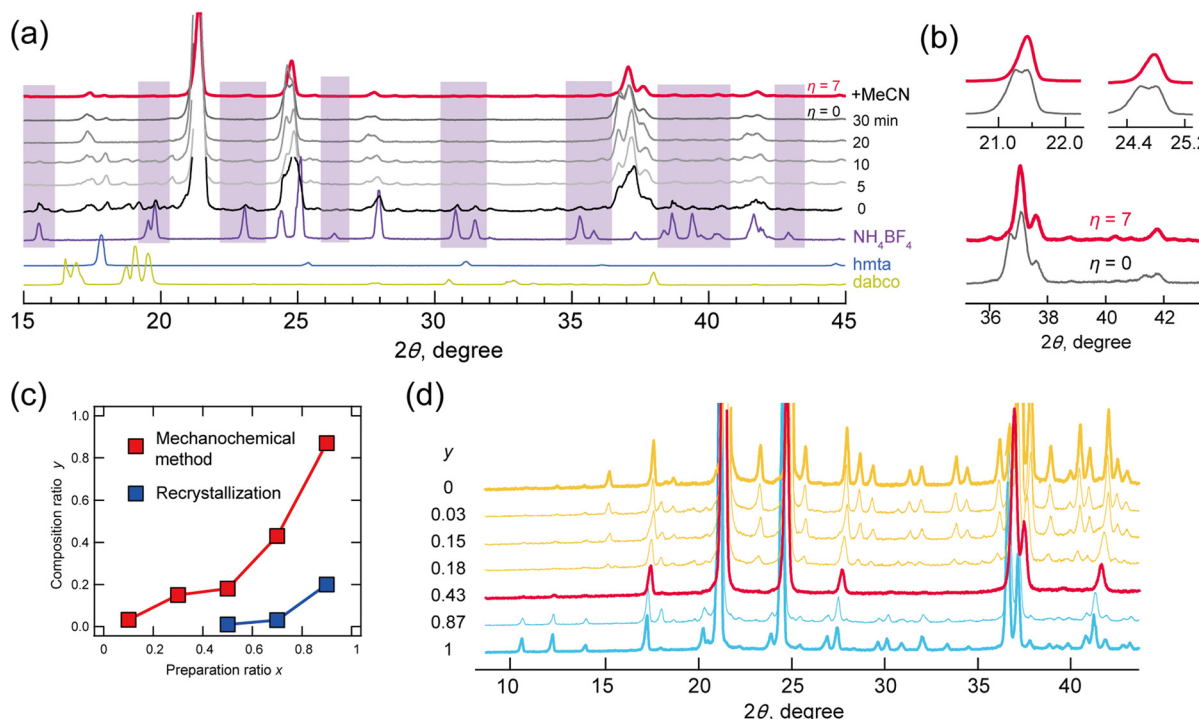


Fig. 1 (a) Time evolution of the P-XRD patterns of solids mixed after grinding for 0, 5, 10, 20 and 30 minutes, and P-XRD pattern of the solid solution prepared by grinding with the addition of acetonitrile for 30 min (black). (b) Extended graph of the P-XRD patterns of $\eta = 0$ and 7. (c) Plots of the mixing ratio x and composition ratio y for mechanochemical (red) and recrystallization (blue) methods. (d) P-XRD patterns of solid solution prepared via mechanochemical methods at variable y .

by Fu *et al.*,^{23,24} which undergoes phase transitions from the ordered phase of space group $Pa\bar{3}$ (phase III) to the PC phase (phase II; $Fm\bar{3}c$) at 333 K, losing the orientational order of H_2dabco^{2+} . The hmta analogue **h**-BF₄ was newly crystallized in the current study and underwent a transition to phase II at 390 K from a tetragonal phase (phase IV; $I4_1/a$).[‡] We successfully crystallized ((d,h)-BF₄) with a wide range of compositions, and the compositional dependence of phase transition behaviour was investigated.

The powder X-ray diffraction (P-XRD) patterns of a mixture of dabco (5.0 mmol), hmta (5.0 mmol), NH₄BF₄ (7.5 mmol), and an aqueous solution of HBF₄ (20.0 mmol) after grinding for 0, 5, 10, 20 and 30 minutes are shown in Fig. 1a. At $t = 0$, diffraction peaks by the perovskite structure were observed in those of NH₄BF₄. With grinding the mixture, the diffraction peaks by NH₄BF₄ disappeared at $t > 20$, indicating that NH₄BF₄ was converted to a perovskite structure. Some diffraction peaks were split however, indicating low structural purity. Mechanochemical synthesis often proceeds *via* the addition of a solvent,^{20,21,25–27} where methods can be classified with parameter η as neat ($\eta = 0$), liquid-assisted grinding ($\eta = 0\text{--}2 \mu\text{L mg}^{-1}$), slurring ($\eta = 2\text{--}12 \mu\text{L mg}^{-1}$), and solution ($\eta > 12$).¹⁷ Parameter η is defined by eqn (1), where V is the amount of solvent (μL) and m is the reactant weight (mg):

$$\eta = V/m \quad (1)$$

In the present study, split diffraction patterns at $\eta = 0$ were improved at $\eta = 7$ *via* the addition of acetonitrile (red line; Fig. 1a and b). Mechanochemical reactions at $\eta = 7$ with

acetonitrile were then performed with various mixing ratios (0.1, 0.3, 0.5, 0.7 and 0.9) for hmta (10x mmol), dabco (10–10x mmol), NH₄BF₄ (10–5x mmol) and HBF₄ (20 mmol). For comparison, the corresponding crystallizations were also performed by dissolving the compounds in water.

The compositions y (dabco; hmta = $1 - y$) in solid solutions were plotted for mechanochemical methods (red) and recrystallization from water (blue) (Fig. 1c). These y values determined by peak area in liquid chromatography–mass spectrometry and elemental analysis were relatively concordant (calibration in Fig. S3-1 (ESI[†]) and experimental results in Tables S3 and S4-1, ESI[†]). In all cases, the y values obtained *via* mechanochemical methods were higher than those obtained *via* recrystallization. This is accounted for by hydrolysis of hmta by an acid. Respective ratios y for mixing ratios x of 0.1, 0.3, 0.5, 0.7, and 0.9 were 0.03, 0.15, 0.18, 0.43 and 0.87. Solid solutions crystallized *via* mechanochemical methods were all-proportional solid solutions.

Fig. 1d shows the P-XRD patterns of solid solutions prepared *via* mechanochemical methods, measured at room temperature. The diffraction patterns of lower hmta contents, $y = 0.03$, 0.15 and 0.18 (indicated by yellow lines in Fig. 1d), corresponded to that of static phase **d**-BF₄ (space group $Pa\bar{3}$, phase III). At $y = 0.43$, the diffraction pattern (indicated by a red line) differed from those of **d**-BF₄ and **h**-BF₄ above 93 K (Fig. S4-1, ESI[†]). This corresponds well with that of their PC phase (phase II; comparisons are shown in Fig. S4-1, ESI[†]). At $y = 0.87$, the diffraction pattern was consistent with that of the static phase of **h**-BF₄ (phase IV). These experimental results indicated the compositional phase transition between **d**-BF₄



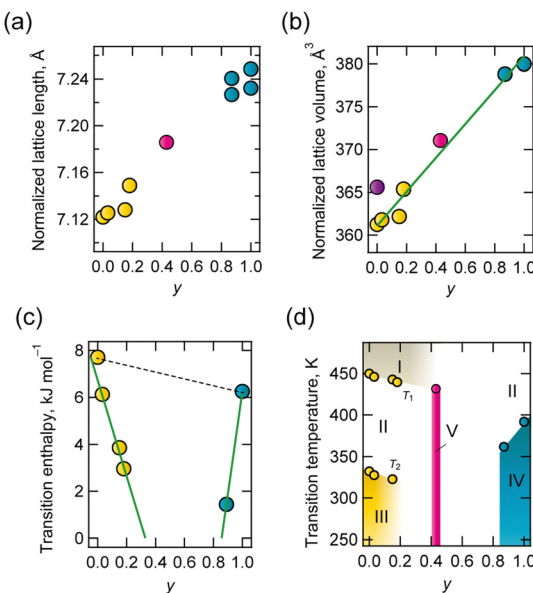


Fig. 2 Component dependence of (a) normalized lattice length, (b) normalized lattice volume (purple circle represents values at phase II of **d**-BF₄), (c) transition enthalpy to phase II from phase III (yellow) or phase IV (blue) and (d) phase diagram.

and **h**-BF₄, where an anomaly phase (phase V) appeared at their boundary $y = 0.43$.

The lattice parameters of solid solutions were evaluated, and the composition dependence of lattice length and volume normalized for the ABX₃ composition is shown in Fig. 2a and b. The lattice dimensions were linearly associated with composition. This is a typical relationship in all-proportional solid solutions, known as Vegard's law.

The respective transition temperatures of **d**-BF₄ and **h**-BF₄ to the PC phase were 332 K and 392 K. Differences in intermolecular interactions and the high symmetry of hmta contribute to higher transition temperatures. Solid state hmta melted at 536 K without a transition to the PC phase, even though dabco transitioned to the PC phase at 351 K before melting (434 K). This is considered to be because highly symmetric hmta has a lower entropy change with respect to transition.²⁸ The results of differential thermal analysis (DTA) and differential scanning calorimetry (DSC) are summarized in Table S4-2 and Fig. S4-2, Fig. S4-3 (ESI†). Thermal anomaly, which indicates a transition to phase II (transition temperature T_2), was observed except for the case $y = 0.43$. At approximately 450 K (transition temperature T_1), thermal anomaly was also observed for $y = 0, 0.03, 0.15, 0.18$ and 0.43 in the DTA chart. This is considered to represent disordering of BF₄⁻ (phase I). The phase transition enthalpy against y is shown in Fig. 2c, and a phase diagram is shown in Fig. 2d. Transition enthalpies and temperature decreased toward $y = 0.43$, at which point the thermal anomaly disappeared in both DSC and DTA.

At the transition from ordered phase III or IV to disordered phase II, the compositional average of enthalpy change, $\Delta H(y)$, is represented by

$$\Delta H(y) = (1 - y)\Delta H(\mathbf{d}\text{-BF}_4) + y\Delta H(\mathbf{h}\text{-BF}_4) \quad (2)$$

with $\Delta H(\mathbf{d}\text{-BF}_4)$ being 7.71 kJ mol⁻¹ and $\Delta H(\mathbf{h}\text{-BF}_4)$ being 6.11 kJ mol⁻¹. This model assumes that H₂hmta²⁺ and H₂dabco²⁺ behave independently at phase transitions. However, experimental values do not follow this model (dotted line in Fig. 2c), indicating that H₂hmta²⁺ and H₂dabco²⁺ are randomly distributed in the solid state, and the thermal motion of each is correlated. We consider that the structural correlation may be due to a structural relationship between the A-site molecule and {NH₄(BF₄)₆} octahedron.

Lattice length and volume were consistent with the compositional average, but their phase transition behaviours were not. In addition, the compositional boundary was observed at $y = 0.43$, where (i) the diffraction pattern was consistent with that of the PC phase of cubic *Fm*̄*3c* above 223 K, but (ii) the thermal anomaly identical to a first-order-type phase transition disappeared. The unit cell volume normalised for composition was 371 Å³ for $y = 0.43$ at room temperature, which is larger than the 367 Å³ of phase II of **d**-BF₄, but smaller than the 395 Å³ of **h**-BF₄. H₂dabco²⁺ molecules at $y = 0.43$ are thus considered to be in enough space to exhibit rotational disorder, but hmtaH₂²⁺ is not. One possible structure proposed at $y = 0.43$ at approximately room temperature is a mixture of static (random) orientational disorder of H₂hmta²⁺ and dynamic disorder of H₂dabco²⁺. Solid-state ¹³C-NMR (nuclear magnetic resonance; Fig. S4-9, ESI†) was characterized for $y = 0.43$, **d**-BF₄ and **h**-BF₄ at 300 K, and the results are summarized in Table S4-1 (ESI†). Peaks for dabco and hmta at $y = 0.43$ were sharper than those associated with **d**-BF₄ and **h**-BF₄. This implies that A-site molecules at $y = 0.43$ are in higher structural symmetry. This is consistent with our structural model.

The dynamics of molecular motion were investigated *via* temperature variable complex permittivity measurements. Solid solution (**d,h**)-BF₄ ($y = 0.03, 0.15, 0.18, 0.43$ and 0.87) exhibited identical frequency and temperature dispersion at 100–300 K (Fig. S4-4 to S4-8, ESI†) due to Debye-type electric dipole relaxation. The corresponding anomaly was not observed for **d**-BF₄, but was observed for **h**-BF₄ in different temperature ranges above 300 K. A plot of activation energy and temperature at 0.01 Hz estimated from the Arrhenius relationship is shown in Fig. 3a. These values were less dependent on composition at 0.3–0.4 eV and ~130 K respectively, indicating that the dipole relaxations have the same origin. In contrast, ε_1 , ε_2 and D ($\equiv \varepsilon_2/\varepsilon_1$) values depend strongly on y . D values at 1 MHz at

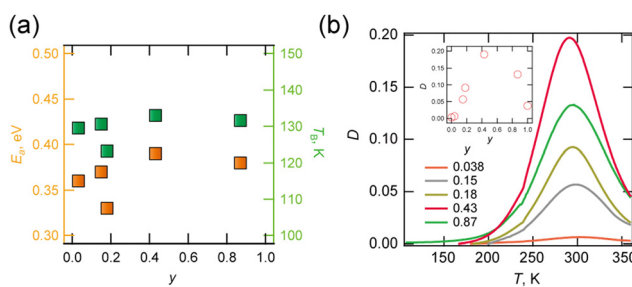


Fig. 3 (a) Plot of activation energy E_a and temperature T_B estimated for $f = 0.01$ Hz via Arrhenius plotting and (b) plot of D against T at variable y (inset: plot of D at 300 K with y).

different y points are shown in Fig. 3b. Peak top temperature did not depend on y , but the peak was largest at $y = 0.43$. We consider that this dipole relaxation originated from the thermal motion of the $\text{H}_2\text{dabco}^{2+}$ and/or $\{\text{NH}_4(\text{BF}_4)_6\}$ octahedron, whose static order melt point is approximately 140 K.

In summary, mechanical methods crystallized all-proportional solid solutions of **d**- BF_4 and **h**- BF_4 . Even though lattice dimensions were proportional to y , the thermodynamic values of phase transition were not. As y increased, unit cell volume exceeded that of PC phase **d**- BF_4 , and the compositional boundary appeared at $y = 0.43$, where highly symmetric cubic-type diffraction was observed above 223 K. We considered the structural mode of the boundary to be a random mixture of thermally dynamic $\text{H}_2\text{dabco}^{2+}$ and orientationally disordered $\text{H}_2\text{hmta}^{2+}$. Phase transition temperature and molecular dynamics strongly depend on the ratio of the two, clearly indicating that solid metal-free perovskite solution is advanced and effective for tuning physical properties, as are traditional perovskites, where mechanical crystallization is a useful technique for all-proportional solid solution. We think that band tuning for optoelectronic properties is also possible because A-site molecules contributed to the electronic state (band gap) of the crystal.²⁹

The authors acknowledge the extensive contribution of Structural Sciences from Leading-Edge Materials to Cultural and Archaeological Works, Yamaguchi University. They also express their gratitude to Mr Matsuoka, Institute of Systems Biology and Radioisotope Analysis, Yamaguchi University, for his valuable advice and support with the analysis of liquid chromatography-mass spectrometry conducted using a Thermo Fisher Orbitrap Exploris 120. The authors acknowledge the financial support from the cooperative research program of the Network Joint Research Centre for Materials and Devices of Japan.

Data availability

https://www.ccdc.cam.ac.uk/structures/ 获得。所有在本研究中生成并分析的数据，包括分析、光谱、晶体学、热学和介电学数据，均包含在本文及其 ESI[†] 中。

Conflicts of interest

无冲突声明。

Notes and references

[‡] **h**- BF_4 从含 hmta 和 HBF_4 的混合水溶液中分离得到（图 S2-1，ESI[†]）。结晶过程和表征的详细信息在 ESI[†] 中包含。在温度可变的单晶 X 射线衍射研究（表 S1）中。

和图 S2-3, S2-4, ESI[†] 和热 DTA (图 S2-5, ESI[†]) 和 DSC (图 S2-6, ESI[†]) 分析中，观察到了从空间群 $I4_1/a$ (有序相) 到 $Fm\bar{3}c$ (PC 无序相) 的相变，其中 A 站分子无序但 BF_4^- 的取向被冻结，观察到在 392 K。在温度和频率依赖性测量中，Debye 型弛豫在 300 K 以上 (图 S2-7, ESI[†])。弛豫活化能估计为 0.78 eV，基于 Arrhenius 图 (图 S2-8, ESI[†])。我们认为这起源于 $\text{H}_2\text{hmta}^{2+}$ 的热无序向 PC 相的转变。

- 1 I. Grinberg, D. V. West, M. Torres, G. Gou, D. M. Stein, L. Wu, G. Chen, E. M. Gallo, A. R. Akbashev, P. K. Davies, J. E. Spanier and A. M. Rappe, *Nature*, 2013, **503**, 509–512.
- 2 X. Hou and J. Yu, *J. Am. Ceram. Soc.*, 2013, **96**, 2218–2224.
- 3 B. Jaffe, R. S. Roth and S. Marzullo, *J. Appl. Phys.*, 1954, **25**, 809–810.
- 4 Z. H. Liu, A. R. Paterson, H. Wu, P. Gao, W. Ren and Z. G. Ye, *J. Mater. Chem. C*, 2017, **5**, 3916–3923.
- 5 W. Q. Liao, D. Zhao, Y. Y. Tang, Y. Zhang, P. F. Li, P. P. Shi, X. G. Chen, Y. M. You and R. G. Xiong, *Science*, 2019, **363**, 1206–1210.
- 6 C. A. Bremner, M. Simpson and W. T. A. Harrison, *J. Am. Chem. Soc.*, 2002, **124**, 10960–10961.
- 7 H. Y. Ye, Y. Y. Tang, P. F. Li, W. Q. Liao, J. X. Gao, X. N. Hua, H. Cai, P. P. Shi, Y. M. You and R. G. Xiong, *Science*, 2018, **361**, 151–155.
- 8 X. Song, Q. Li, J. Han, C. Ma, Z. Xu, H. Li, P. Wang, Z. Yang, Q. Cui, L. Gao, Z. Quan, S. F. Liu and K. Zhao, *Adv. Mater.*, 2021, **33**, e2102190.
- 9 H. S. Wu, B. T. Murti, J. Singh, P. K. Yang and M. L. Tsai, *Adv. Sci.*, 2022, **9**, 2104703.
- 10 X. Song, G. Hodes, K. Zhao and S. F. Liu, *Adv. Energy Mater.*, 2021, **11**, 2003331.
- 11 Z. Z. Li, G. Q. Peng, Z. H. Li, Y. K. Xu, T. Wang, H. X. Wang, Z. T. Liu, G. Wang, L. M. Ding and Z. W. Jin, *Angew. Chem., Int. Ed.*, 2023, **62**, e202218349.
- 12 X. Song, T. Li, H. Li, S. Lin, J. Yin and K. Zhao, *Sci. China Mater.*, 2024, **67**, 1348–1355.
- 13 H. Morita, R. Tsunashima, S. Nishihara, K. Inoue, Y. Omura, Y. Suzuki, J. Kawamata, N. Hoshino and T. Akutagawa, *Angew. Chem., Int. Ed.*, 2019, **58**, 9184–9187.
- 14 H. Morita, R. Tsunashima, S. Nishihara and T. Akutagawa, *CrystEngComm*, 2020, **22**, 2279–2282.
- 15 T. Seo, N. Toyoshima, K. Kubota and H. Ito, *J. Am. Chem. Soc.*, 2021, **143**, 6165–6175.
- 16 G. W. Wang, K. Komatsu, Y. Murata and M. Shiro, *Nature*, 1997, **387**, 583–586.
- 17 T. Friščić, C. Mottillo and H. M. Titi, *Angew. Chem.*, 2020, **132**, 1030–1041.
- 18 F. Lyu, Z. Chen, R. Shi, J. Yu and B. L. Lin, *J. Solid State Chem.*, 2021, **304**, 122548.
- 19 A. Karmakar, A. M. Askar, G. M. Bernard, V. V. Terskikh, M. Ha, S. Patel, K. Shankar and V. K. Michaelis, *Chem. Mater.*, 2018, **30**, 2309–2321.
- 20 M. Lusi, I. J. Vitorica-Yrezabal and M. J. Zaworotko, *Cryst. Growth Des.*, 2015, **15**, 4098–4103.
- 21 E. Batisai, M. Lusi, T. Jacobs and L. J. Barbour, *Chem. Commun.*, 2012, **48**, 12171–12173.
- 22 R. Tsunashima, *CrystEngComm*, 2022, **24**, 1309–1318.
- 23 G. Z. Liu, J. Zhang and L.-Y. Wang, *Synth. React. Inorg., Met.-Org., Nano-Met. Chem.*, 2011, **41**, 1091–1094.
- 24 L. L. Chu, T. Zhang, W. Y. Zhang, P. P. Shi, J. X. Gao, Q. Ye and D. W. Fu, *J. Phys. Chem. Lett.*, 2020, **11**, 1668–1674.
- 25 E. Schur, E. Nauha, M. Lusi and J. Bernstein, *Chemistry*, 2015, **21**, 1735–1742.
- 26 B. Saikia, A. Seidel-Morgenstern and H. Lorenz, *Cryst. Growth Des.*, 2021, **21**, 5854–5861.
- 27 D. Braga, L. Maini and F. Grepioni, *Chem. Soc. Rev.*, 2013, **42**, 7638–7648.
- 28 L. N. Becka and D. W. J. Cruickshank, *Proc. R. Soc. London, Ser. A*, 1963, **273**, 435–454.
- 29 J. Bie, D. B. Yang, M. G. Ju, Q. Pan, Y. M. You, W. Fa, X. C. Zeng and S. Chen, *JACS Au*, 2021, **1**, 475–483.

